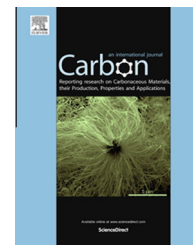


Available at [www.sciencedirect.com](http://www.sciencedirect.com)

ScienceDirect

journal homepage: [www.elsevier.com/locate/carbon](http://www.elsevier.com/locate/carbon)

# Spin lifetime of itinerant electrons in chemically synthesized graphene multi-layers



Bálint Náfrádi <sup>a,\*</sup>, Mohammad Choucair <sup>b</sup>, László Forró <sup>a</sup>

<sup>a</sup> Institute of Physics of Complex Matter, EPFL, Lausanne, Switzerland

<sup>b</sup> School of Chemistry, University of Sydney, Sydney 2006, Australia

## ARTICLE INFO

### Article history:

Received 21 January 2014

Accepted 25 March 2014

Available online 1 April 2014

## ABSTRACT

A chemically synthesized graphitic material where the structural coherence between the layers is missing approximates very well the assembly of graphene sheets. Our multi-frequency (9.4–420 GHz) electron spin resonance (ESR) study clearly identifies itinerant and localized electrons below 50 K. The metallic signal ascribed to the conduction electrons in graphene is characterized by a remarkably long spin lifetime of 65 ns. Above this temperature incoherent in-plane and inter-plane scattering give a motionally narrowed single line at  $g = 2.0044$ .

© 2014 Elsevier Ltd. All rights reserved.

## 1. Introduction

A materials' utility for spintronic and spin quantum computing applications relies on two parameters, the spin relaxation time  $T_S$  and the spin diffusion length  $l_S = (D \cdot T_S)^{1/2}$ , where  $D$  is the diffusion coefficient. Increasing  $T_S$  permits the manipulation of coherent spin, while long  $l_S$  enables information transport without significant loss. Graphene has been proposed as an ideal platform for spintronic and spin quantum computing applications due to the long  $T_S$  expected from the small spin-orbit coupling of carbon atoms and the weak hyperfine interactions resulting from the absence of nuclear spins for the main  $^{12}\text{C}$  isotope. Indeed, very long  $l_S$  in the 100  $\mu\text{m}$ , much longer than those in conventional metals and semiconductors, have been observed [1]. However, values of  $l_S$  have been reported to vary over the 2–100  $\mu\text{m}$  range [1–3]. Moreover, the current achievable  $T_S$  values for graphene are limited to within the 0.2–2.3 ns range [2,4–6].

The origin of  $T_S$  and  $l_S$  values for graphene remain controversial due to paralleling works performed on carbon nanotubes [7–10] and the proposed influence of graphene

morphology [11,12]. Indeed, intricate spin architectures and the structural tuning of magnetic properties have been enabled using graphene nanoribbon widths and edges [13] and promising spintronic devices have been recently crafted using graphenic components [14]. With the development of novel synthetic pathways to graphenic architectures [15–17] and of various chemical methods for the large scale production of graphene [18], the rich interaction-induced phenomena that exists between multiple stacked layers can now be explored. For example, slightly rotated graphene sheets can be responsible for electrical decoupling between the layers, even though they are vertically separated by sub-nanometer distances [19,20].

Identification of the intrinsic  $T_S$  and  $l_S$  of graphene using spin transport devices arrives at notable drawbacks in the use of metallic ferromagnetic contacts [3,21]. Electron spin resonance (ESR) spectroscopy is an ideally suited contactless method to determine spin transport parameters. ESR spectroscopy can be used as a sensitive probe of the specific atomic nature of point defects and various localized and itinerant spin states in carbon materials [22–29]. Weakly interacting

\* Corresponding author.

E-mail address: [nafradi@yahoo.com](mailto:nafradi@yahoo.com) (B. Náfrádi).

<http://dx.doi.org/10.1016/j.carbon.2014.03.046>

0008-6223/© 2014 Elsevier Ltd. All rights reserved.

spin systems like those commonly found in carbon materials can often result in observations of coupled ESR [22,30,31]. Despite this, several ESR studies have reported carbon-based materials that reveal the presence of a conduction electron [9,22,24,26,28,29,32–36]. The studies reporting conduction electron spin resonance (CESR) in carbon materials detail interactions through bundling [9,23,28], peeling [37], or mobile in-plane  $\pi$ -electrons of graphene [22,32]. In the case of narrowed graphene materials like nanoribbons, direct evidence of a delocalized transition has yet to be observed; hindered due to an intrinsically small  $g$ -factor anisotropy which often limits the spectroscopic information that can be obtained by conventional low-frequency ESR. Alternatively, high-frequency ESR is able to provide detailed spectroscopic information capable of distinguishing the strength of interactions between different spin systems present in a material [38–41].

Here, we study an assembly of chemically synthesized graphene sheets as a model system, which represents both locally high quality graphene and disorder on large scales. By our high frequency ESR (up to 420 GHz) we can deconvolute the two contributions below 50 K arising from conduction electrons and localized spins. In graphene the spin lifetime of conduction electrons is unprecedentedly long, 65 ns. This corresponds to tens of  $\mu\text{m}$  of spin diffusion length. Above 50 K, the conduction electrons and the localized spins start to interact strongly. Although the motionally narrowed common ESR line gives nominally an even longer lifetime, this cannot be used for spintronic application since it corresponds to localized charges.

## 2. Experimental

To obtain the graphene material we employed a method based on solvothermal synthesis known to produce 3-dimensional networks of graphene [42]. The term ‘solvothermal’ denotes conditions involving reactions performed at a temperature above the boiling point of a solvent in a closed reaction vessel. In this case propanol was used as the alcohol feedstock for the solvothermal reaction with sodium metal at 493 K for 72 h. The solvothermal reaction produced a solid product which was rapidly pyrolysed. The resulting carbon material was washed with water, then with acidified ethanol (2 M hydrochloric acid in ethanol, 1:4 vol./vol. ratio), and filtered under dynamic vacuum before drying in a vacuum oven at 473 K for 1 h.

Transmission electron microscopy (TEM) shows that the material is dominated by extended networks of fused graphene sheets in addition to large fragmented sections spanning micrometer length scales, Fig. 1 (see also Supporting Information S1). It is important to note that washing the graphene material by stirring, and mild sonication treatments, are known to disrupt the weakly fused graphene structure to obtain free sheets [43]. Selected area electron diffraction (SAED) patterns of various graphene regions were indicative of a polycrystalline material, Fig. 1b. From direct observation under the TEM, we realize that the polycrystalline patterns represent a combination of (i) layers of graphene with a small degree of angular offset (i.e. twisting) with no inter-planar correlation and (ii) graphene with in-plane poly-crystalline

domains. Primary graphitic features relating to (ABAB..) stacking were absent with the exception of a (112) reflection; this may arise due to the graphene displaying slight twists and folds as further evidenced by high resolution TEM images in Fig. 1.

ESR spectroscopy in the 9.4–420 GHz frequency-range was performed in the 2–300 K range. At 9.4 GHz a commercial spectrometer was used. In the millimeter wave range experiments were carried out on a home-made 105–420 GHz quasi optical spectrometer. More details about the spectrometers can be found in previous works [44,45]. Conventional low power first-derivative-absorption spectra were detected through applying sinusoidal modulation of the externally applied magnetic field with incident microwave power as well as the modulation amplitude cautiously reduced to avoid signal distortion. The ESR line-width ( $\Delta H$ ),  $g$ -factor, and spin susceptibility,  $\chi$ , were quantified by least square fitting of the derivative absorption spectra. The absolute value of  $\chi$  was determined by a calibrated  $\text{CuSO}_4 \times 5\text{H}_2\text{O}$  reference sample [46].

## 3. Results and discussion

At room temperature the 9.4 GHz ESR signal of the graphenic material has a highly symmetric Lorentzian shape at  $g = 2.0044$  position with  $\Delta H = 0.046$  mT line-width (see Supporting Information S2). The spin concentration is  $\chi = 3.7 \times 10^{19}$  spin/g assuming spin-1/2 paramagnetic moments. The average spin-spin distance,  $r_{e-e}$ , while assuming non-correlated defect sites and thus a Poisson distribution for defects, equates to  $0.55N_e^{-1/3} = 1.3$  nm (where  $N_e$  is the spin concentration). Remarkably, this  $r_{e-e}$  would be expected to induce an ESR line-width of  $\Delta H_{\text{dip-dip}} = 0.87$  mT, solely by the dipole-dipole interaction between nearest neighbor spins [47]. This corresponding line-width is about 20 times broader than the experimentally observed one. Moreover, the dipole-dipole interaction is only a lower bound for the ESR line-width of insulating carbon nanostructures; unresolved hyperfine interactions and other anisotropies can, in principle, further broaden the line [22,24]. Thus, a narrowing mechanism is required to be present in the system to describe the observed externally narrow ESR line-width. Due to the large  $r_{e-e}$ , exchange-narrowing between paramagnetic defects can be excluded, and therefore itinerant conduction electrons play a crucial role in the motional narrowing of the ESR line-width. Furthermore, it should be emphasized that the line-width of  $\Delta H = 0.046$  mT at 300 K nominally gives a spin lifetime of 160 ns but this cannot be useful for spintronics applications since it corresponds to paramagnetic localized spins.

In order to gain more insight to the narrowing mechanism and to the coupling of the paramagnetic and conduction electrons we performed high-frequency ESR in the 105–420 GHz frequency range at  $T = 300$  K. The two spin systems, i.e. the localized and the delocalized, are observable independently by ESR if the energy separation,  $(g_{\text{loc}} - g_{\text{CESR}})\mu_B B_0$ , exceeds the interaction strength between the two spin systems. Indeed, our high-frequency ESR experiments at 300 K revealed a linear broadening of the spectral line as a function of frequency,  $\omega$ . The frequency dependence follows

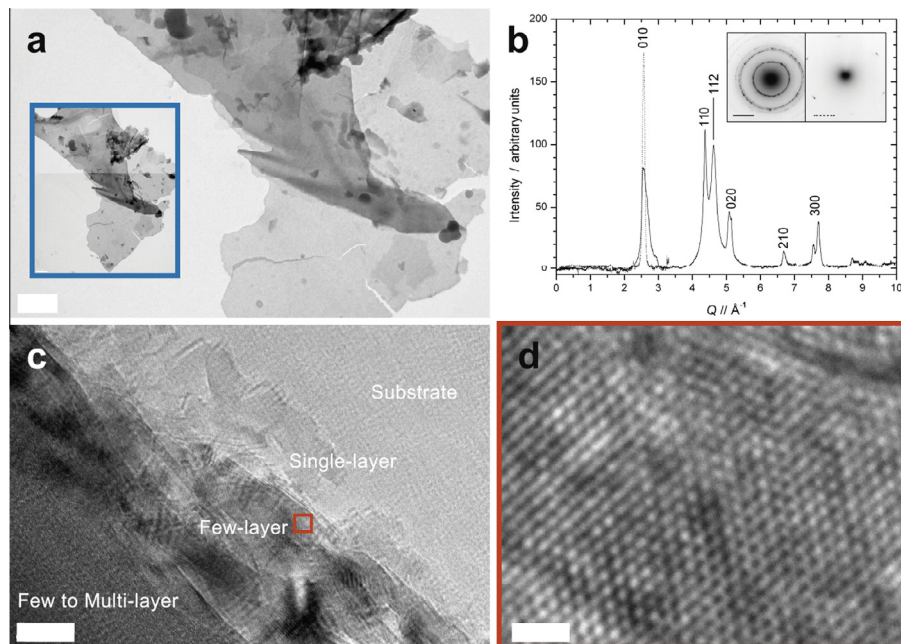


**Fig. 1 – (a)** A fragmented graphene region which has broken from the extended network. The graphene material is layered as evidenced by regions of relative opacity. The graphene folds, bends, crumples, twists, and has long (>1  $\mu\text{m}$ ) cracks. Inset in (a) is the superposition of two images of the same graphene fragment taken at the same magnification to illustrate the extensive nature of the chemically derived graphene that spans across  $10\ \mu\text{m} \times 5\ \mu\text{m}$  (also see Supporting Information S1). **(b)** Background-corrected electron diffraction plot of selected regions in the graphene material integrated along the  $(hk0)$  directions, having  $d$ -spacing of  $\sqrt{3}/n$ . Inset: SAED patterns of the two regions containing graphene material taken with focal length (left) 950 mm and (right) 2400 mm. **(c)** The relative opacity of an increasing number of randomly offset layers of different size obstructs attempts to resolve the graphene lattice. **(d)** A highly resolved image of a region in (c) showing the hexagonal  $sp^2$  network; the material is not amorphous. Scale bars represent in (a) 500 nm, (c) 10 nm, and (d) 1 nm. (A colour version of this figure can be viewed online.)

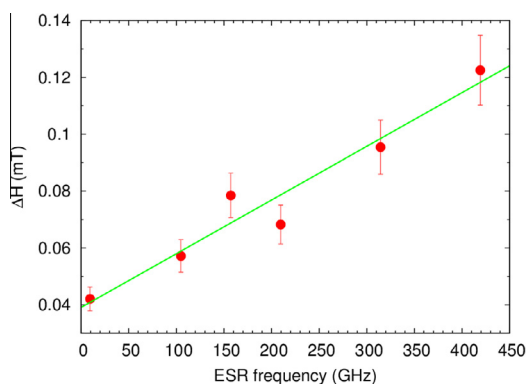


**Fig. 2 – Frequency dependency of the ESR line-width at  $T = 300\ \text{K}$ . Line is result of a least square linear fit to  $\Delta H = \Delta H_0 + b \cdot \omega$  with parameters  $\Delta H_0 = 0.039\ \text{mT}$  and  $b = 1.9 \times 10^{-4}\ \text{mT/GHz}$ . (A colour version of this figure can be viewed online.)**

the form of  $\Delta H = \Delta H_0 + b \cdot \omega$  with parameters  $\Delta H_0 = 0.039\ \text{mT}$  and  $b = 1.9 \times 10^{-4}\ \text{mT/GHz}$ , Fig. 2. However, the ESR line maintained a highly symmetric Lorentzian line-shape and the  $g$ -factor was also independent of frequency. We can attribute the broadening of the line to an unresolved  $g$ -factor anisotropy that is motional averaged by conduction electrons.

The motional narrowing becomes progressively less efficient with increasing frequency due to the finite  $g$ -factor anisotropy; although, 420 GHz is not sufficient to split the spectral lines at 300 K. We note, that the observed field induced broadening  $b$  is about 30 times smaller than in the case of insulating graphene ribbons [24], indicating the strong role of conduction electrons in motional narrowing.

The presence of itinerant electrons is further supported by temperature dependent experiments presented in Figs. 3 and 4. The ESR line-shape is always Lorentzian at 9.4 GHz. The convoluted temperature behavior of the spin susceptibility measured at 9.4 GHz is incompatible with a simple isolated dangling bond as the origin of the ESR signal, Fig. 3a. A Curie–Weiss fit reveals paramagnetic behavior above 60 K with negligible – about 4 K – Weiss temperature. At 50 K there is an abrupt change in the temperature dependence of the susceptibility. Below this temperature the Curie constant drops by a factor of 4, and a small Pauli like temperature independent metallic behavior appears (clearly visible in the inset to Fig. 3a). The Pauli contribution is  $\chi_{\text{Pauli}} = 3.1 \times 10^{-7}\ \text{emu/g}$  by normalizing to the entire sample mass (about 4% of the low temperature saturation susceptibility). The corresponding electron density is  $n \sim 1.44 \times 10^{10}\ \text{cm}^{-2}$ . This value is about an order of magnitude lower than the finite  $T = 0$  charge density inhomogeneity  $n_0 \sim 1.5\text{--}3 \times 10^{11}\ \text{cm}^{-2}$  due to electron–hole puddles [20,48,49]. The puddles are expected to set the mini-

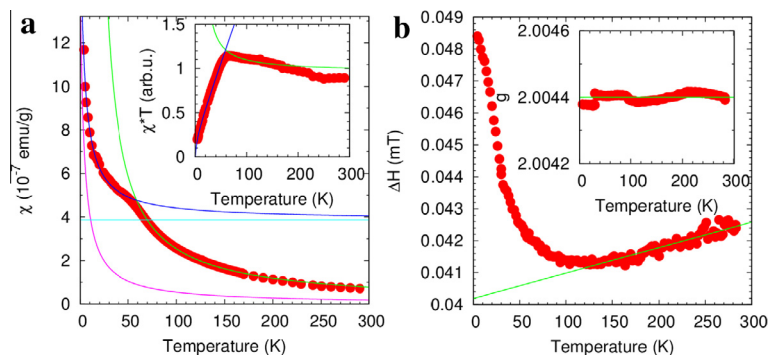


**Fig. 3 – (a) Temperature dependence of the spin susceptibility measured at 9.4 GHz. Inset in (a) presents  $\chi T$  as a function of temperature; blue and green lines are results of a Curie–Weiss fit considering data points above and below 60 K respectively. At high-temperatures the susceptibility is paramagnetic. At low temperatures it is a superposition of a temperature independent metallic and a paramagnetic component. (b) The ESR line-width as a function of temperature measured at 9.4 GHz. At high temperatures the line-width decreases monotonically while it increases rapidly at low temperatures. Inset in (b) shows the temperature independence  $g$ -factor and lines of linear fits to the data. (A colour version of this figure can be viewed online.)**

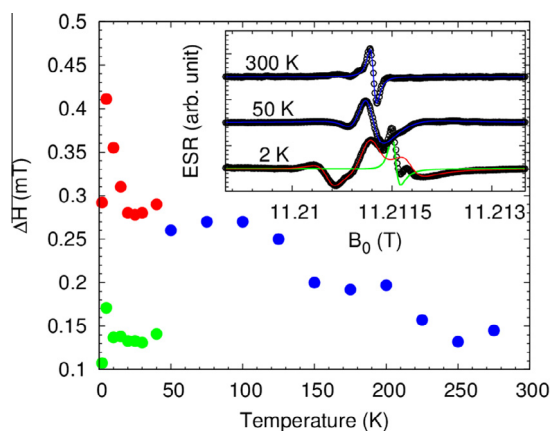


**Fig. 4 – Temperature dependence of the ESR line-width measured at 315 GHz Larmor frequency. At high-temperatures above 50 K a single motional narrowed line is observed (blue symbols). Below 50 K (red symbols) represent the paramagnetic line-width, a CCSR line appears at the same temperature with temperature independent line-width (green symbols). The inset shows a typical spectrum recorded at 300 K and at 50 K above the transition with the blue lines tracing fits to a Lorentzian profile. The lower trace in the inset shows spectrum recorded at 2 K with fits to the narrow CCSR line shown in green and paramagnetic powder spectra shown in red. (A colour version of this figure can be viewed online.)**

mal achievable carrier density of graphenic sheets. The small overall number is partly due to the fact that the signal was normalized to the whole mass of the sample but may also be an intrinsic property [50].

The temperature dependence of the line-width exhibits an anomaly similar to the spin susceptibility below 70 K, Fig. 3b. The line-width decreases linearly with decreasing temperature between 120–300 K. Below 70 K the line-width starts to increase with further decreasing temperatures. The  $g$ -factor

is temperature independent within experimental accuracy over the entire temperature range (inset in Fig. 3b).

The results indicate that localized paramagnetic centers, dangling bonds, and itinerant conduction electrons are present in the sample. Furthermore these spin systems are coupled. The Lorentzian line-shape, the linearity in temperature decrease of the ESR line-width, and the paramagnetic temperature dependence of the susceptibility indicate the bottleneck effect in the spin relaxation at high temperatures [22]. We attribute the anomaly below 70 K in both the spin susceptibility and ESR line-width to temperature induced decoupling of the localized and conduction electrons. It has been shown by pulsed ESR experiments at  $\sim 9$  GHz that localized defect sites alone exhibit a significantly broadened inhomogeneous ESR line [22,24]. This broad line dominates the low-frequency ESR at low temperatures. Since there is no observable anomaly in the  $g$ -factor, the decoupled paramagnetic ESR and CCSR are overlapping at this frequency. Indeed at low temperatures the signal asymmetry increased slightly but no splitting of the spectral lines was observed.

In contrast to 9.4 GHz ESR the decoupling of itinerant and localized spins is clearly observable at 315 GHz. The temperature dependence of the ESR line-width at 315 GHz frequency shows a weak increase with decreasing temperature at high temperatures, Fig. 4. A spectra characteristic to powdered material gradually develops with extremely small  $g$ -factor anisotropy as the temperature is decreased. A new line with CCSR properties appears in the 315 GHz spectra below 50 K. The inset of Fig. 4 shows typical spectra below and above 50 K. At low temperatures a paramagnetic ‘powder-like spectra’ with  $g_{xx} = 2.00441$ ,  $g_{yy} = 2.00452$ ,  $g_{zz} = 2.00431$ , and an isotropic CCSR line with  $g_{\text{CESR}} = 2.00434$  is observable simultaneously. This temperature is in good agreement with the 9.4 GHz observations where the temperature independent CCSR behavior emerged below 50 K.

The broadening of the paramagnetic line above 50 K and a smooth development of the ‘powder-like spectra’ is also in accord with the gradual decoupling of itinerant and localized spins observed at 9.4 GHz. The spin susceptibility of the CCSR

line is about 8% relative to the paramagnetic signal, which is in good agreement with the 9.4 GHz results. The line we assigned to CESR shows temperature independent line-width,  $g$ -factor, and susceptibility, testifying its metallic origin. Remarkably the  $\Delta H_{\text{CESR}}$  (0.1 mT) observed below 50 K yields a 65 ns spin lifetime when assuming that the spin–spin and spin–lattice relaxation times are equal ( $T_1 = T_2$ ) [22]. The Pauli spin susceptibility of the CESR signal corresponds to a density of states of about  $5 \times 10^{-2}$  states/eV atom (assuming linear graphene like dispersion), which is about six times smaller than that of  $\text{KC}_8$  [46].

The temperature regime of the decoupling, i.e. below  $\sim 70$  K, where electronic and thermo-electric anomalies are commonly observed due to the disappearance of thermally excited phonons, indicates that phonons play a crucial role [51]. The decreasing line-width with decreasing temperature observed at 9.4 GHz can be also explained by considering the disappearance of thermally excited phonons active at high temperature. Based on these arguments and the absence of the ABAB stacking, as well as the slight twisting of adjacent layers of the graphenic structure (Fig. 1) we assume that at high-temperatures interlayer hopping conduction is mediated by phonons in agreement with earlier transport studies [20,49].

We propose that the spectral line broadening is due to decreased  $T_2$  during interlayer electron diffusion. Phonons destroy the spin-phase coherence between the layers, while mediating electronic transport, thus broadening the CESR line beyond observation. Indeed calculation based on the low temperature  $T_1 = 65$  ns and by our ESR detection limit of 1 mT at 300 K yields  $T_2 < 10^{-11}$  s, which is in the expected limit for the interlayer equilibrium time of  $10^{-6}$ – $10^{-12}$  s [19,20]. By decreasing the temperature and thus dampening the phonon population, conduction electrons become confined over individual graphene layers. The spin–spin relaxation time increases and an observable CESR with temperature independent Pauli-susceptibility (density of states ca.  $5 \times 10^{-2}$  states/eV atom) develops. The overlap between delocalized electrons and static paramagnetic defects decreases in the metallic state thus the motional averaging also becomes less effective at low temperatures and a broadening of the paramagnetic line is observed upon decreasing temperatures.

#### 4. Conclusion

In summary, our results have provided new insights into the fundamental understanding of strongly correlated interactions between multiple spin systems in chemically derived graphene. We have shown that a single averaged ESR line originating from an assembly of graphene sheets can be resolved at high frequencies and low temperatures to reveal paramagnetic and CESR contributions. The average spin–spin distance was found to be 1.3 nm associated with an incredibly narrow line width. The results highlight the central role of itinerant conduction electrons when considering the spin dynamics in graphene systems. Approaches linking processable graphene architectures to variations in electron behavior could have vast implications, e.g., from our results the spin lifetime based on the low-temperature narrow line-width of

the CESR ( $\Delta H_{\text{CESR}} = 0.14$  mT) was found to be remarkably long at 65 ns [6,22]. This is in the range required for spintronics applications. Moreover ESR spectroscopy indicates that not only the in-plane but also the inter-plane spin transport should be tailored for spintronics.

#### Acknowledgements

M.C. acknowledges financial assistance from The University of Sydney and technical support from the Australian Centre for Microscopy and Microanalysis. Work at Lausanne was supported by the Swiss National Science Foundation.

#### Appendix A. Supplementary data

Supplementary data associated with this article can be found, in the online version, at <http://dx.doi.org/10.1016/j.carbon.2014.03.046>.

#### REFERENCES

- [1] Dlubak B, Martin M-B, Deranlot C, Servet B, Xavier S, Mattana R, et al. *Nat Phys* 2012;8(7):557–61.
- [2] Han W, Pi K, McCreary KM, Li Y, Wong JJI, Swartz AG, et al. *Phys Rev Lett* 2010;105(16):167202.
- [3] Krompiewski S. *Nanotechnology* 2012;23(13):135203.
- [4] Mani RG, Hankinson J, Berger C, de Heer WA. *Nat Commun* 2012;3:996.
- [5] Tombros N, Jozsa C, Popinciuc M, Jonkman HT, van Wees BJ. *Nature* 2007;448(7153):571–4.
- [6] Yang TY, Balakrishnan J, Volmer F, Avsar A, Jaiswal M, Samm J, et al. *Phys Rev Lett* 2011;107(4):21.
- [7] Corzilius B, Gembus A, Weiden N, Dinse KP, Hata K. *Phys Status Solidi* 2006;243(13):3273–6.
- [8] Dóra B, Gulácsi M, Koltai J, Zólyomi V, Kürti J, Simon F. *Phys Rev Lett* 2008;101(10):106408.
- [9] Beuneu F, L'Huillier C, Salvétat JP, Bonard JM, Forró L. *Phys Rev B* 1999;59(8):5945–9.
- [10] Galambos M, Fábrián G, Simon F, Ćirić L, Forró L, Korecz L, et al. *Phys Status Solidi B* 2009;246(11–12):2760–3.
- [11] Wunsch B, Stauber T, Sols F, Guinea F. *Phys Rev Lett* 2008;101(3):036803.
- [12] Muñoz-Rojas F, Fernández-Rossier J, Palacios JJ. *Phys Rev Lett* 2009;102(13):136810.
- [13] Yazyev OV. *Acc Chem Res* 2013;3:3.
- [14] Wang WH, Han W, Pi K, McCreary KM, Miao F, Bao W, et al. *Appl Phys Lett* 2008;93(18):183107-3.
- [15] Ritter KA, Lyding JW. *Nat Mater* 2009;8(3):235–42.
- [16] Li X, Wang X, Zhang L, Lee S, Dai H. *Science* 2008;319(5867):1229–32.
- [17] Ricco M, Pontiroli D, Mazzani M, Choucair M, Stride JA, Yazyev OV. *Nano Lett* 2011;11(11):4919–22.
- [18] Park S, Ruoff RS. *Nat Nano* 2009;4(4):217–24.
- [19] Bistrizter R, MacDonald AH. *Phys Rev B* 2010;81(24):245412.
- [20] Kim Y, Yun H, Nam S-G, Son M, Lee DS, Kim DC, et al. *Phys Rev Lett* 2013;110(9):096602.
- [21] Jayasekera T, Kong BD, Kim KW, Buongiorno Nardelli M. *Phys Rev Lett* 2010;104(14):146801.
- [22] Augustyniak-Jabłokow MA, Tadyszak K, Maćkowiak M, Lijewski S. *Chem Phys Lett* 2013;557:118–22.
- [23] Ishii S, Miyamoto K, Oguri N, Horiuchi K, Sasaki T, Aoki N, et al. *Physica E* 2003;19(1–2):149–52.

- [24] Rao SS, Stesmans A, van Tol J, Kosynkin DV, Higginbotham-Duque A, Lu W, et al. *ACS Nano* 2012;6(9):7615–23.
- [25] Ćirić L, Sienkiewicz A, Djokić DM, Smajda R, Magrez A, Kaspar T, et al. *Phys Status Solidi B* 2010;247(11–12):2958–61.
- [26] Wagoner G. *Phys Rev* 1960;118(3):647–53.
- [27] Ćirić L, Sienkiewicz A, Náfrádi B, Mionić M, Magrez A, Forró L. *Phys Status Solidi B* 2009;246(11–12):2558–61.
- [28] Náfrádi B, Nemes NM, Fehér T, Forró L, Kim Y, Fischer JE, et al. *Phys Status Solidi B* 2006;243(13):3106–10.
- [29] Szirmai P, Fábíán G, Koltai J, Náfrádi B, Forró L, Pichler T, et al. *Phys Rev B* 2013;87(19):195132.
- [30] Antal Á, Fehér T, Tátrai-Szekeres E, Fülöp F, Náfrádi B, Forró L, et al. *Phys Rev B* 2011;84(7):075124.
- [31] Antal Á, Fehér T, Náfrádi B, Gaál R, Forró L, Jánossy A, et al. *Physica B* 2010;405(11):S168–71. Supplement.
- [32] Dóra B, Murányi F, Simon F. *EPL (Europhysics Letters)* 2010;92(1):17002.
- [33] Ghosh A, Pinto JW, Frota HO. *J Magn Reson* 2013;227:87–92.
- [34] Matsubara K, Tsuzuku T, Sugihara K. *Phys Rev B Condens Matter* 1991;44(21):11845–51.
- [35] Blinc R, Cevc P, Arčon D, Zalar B, Zorko A, Apih T, et al. *Phys Status Solidi B* 2006;243(13):3069–72.
- [36] Blinc R, Arcon D, Cevc P, Pocsik I, Koos M, Trontelj Z, et al. *J Phys: Condens Matter* 1998;10(30):6813.
- [37] Rao SS, Stesmans A, Kosynkin DV, Higginbotham A, Tour JM. *New J Phys* 2011;13(11):113004.
- [38] Náfrádi B, Antal Á, Pásztor Á, Forró L, Kiss LF, Fehér T, et al. *J Phys Chem Lett* 2012;3(22):3291–6.
- [39] Náfrádi B, Olariu A, Forró L, Mézière C, Batail P, Jánossy A. *Phys Rev B* 2010;81(22):224438.
- [40] Nagy KL, Náfrádi B, Kushch ND, Yagubskii EB, Herdtweck E, Fehér T, et al. *Phys Rev B* 2009;80(10):104407.
- [41] Olariu A, Náfrádi B, Ćirić L, Nemes NM, Forró L. *Phys Status Solidi B* 2008;245(10):2029–33.
- [42] Choucair M, Thordarson P, Stride JA. *Nat Nano* 2009;4(1):30–3.
- [43] Choucair M, Tse NMK, Hill MR, Stride JA. *Surf Sci* 2012;606(1–2):34–9.
- [44] Náfrádi B, Gaál R, Fehér T, Forró L. *J Magn Reson* 2008;192(2):265–8.
- [45] Náfrádi B, Gaál R, Sienkiewicz A, Fehér T, Forró L. *J Magn Reson* 2008;195(2):206–10.
- [46] Szirmai P, Fábíán G, Dóra B, Koltai J, Zólyomi V, Kürti J, et al. *Phys Status Solidi B* 2011;248(11):2688–91.
- [47] Van Vleck JH. *Phys Rev* 1948;74(9):1168–83.
- [48] Martin J, Akerman N, Ulbricht G, Lohmann T, Smet JH, von Klitzing K, et al. *Nat Phys* 2008;4(2):144–8.
- [49] Xue J, Sanchez-Yamagishi J, Bulmash D, Jacquod P, Deshpande A, Watanabe K, et al. *Nat Mater* 2011;10(4):282–5.
- [50] Hernandez, Y. R.; Schweitzer, S.; Kim, J.-S.; Patra, A. K.; Englert, J.; Lieberwirth, I.; Liscio, A.; Palermo, V.; Feng, X.; Hirsch, A.; Kläui, M.; Müllen, K., Turbostratic graphitic microstructures: electronically decoupled multilayer graphene devices with robust high charge carrier mobility. In arXiv:1301.6087: 2013.
- [51] Takezawa T, Tsuzuku T, Ono A, Hishiyama Y. *Philos Mag* 1969;19(159):623–8.